



Article

Developing a New Vegetation Index Using Cyan, Orange, and Near Infrared Bands to Analyze Soybean Growth Dynamics

Roger A. Rojas Vásquez¹, Muditha K. Heenkenda^{2,*}, Reg Nelson² and Laura Segura Serrano¹

¹ Department of Agricultural Engineering, Tecnológico de Costa Rica, Cartago 30101, Costa Rica; rogerrojas@estudiantec.cr (R.A.R.V.); lsegura@itcr.ac.cr (L.S.S.)

² Department of Geography and the Environment, Lakehead University, Thunder Bay, ON P7B 5E1, Canada; rjnelson@lakeheadu.ca

* Correspondence: muditha.heenkenda@lakeheadu.ca; Tel.: +1-807-343-8010 (ext. 8746)

Abstract: Remote sensing Vegetation Indices (VIs) are simple, effective, and widely used methods for quantitative and qualitative analysis of vegetation cover, vigor, and growth dynamics. This study developed and assessed a new vegetation index (VI) using Cyan, Orange, and Near Infrared (NIR) bands to assess Soybean growth dynamics. The study was conducted at Lakehead University Agriculture Research Station, Thunder Bay, Canada, over four reproductive stages of Soybean growth (R4–R7). Spectral profiles were created for each stage, and the correlation between each spectral band at different stages was tested. There was no linear correlation between different bands except the correlation between the Cyan and Orange bands at R5 and R6 stages. Existing VIs have also been explored using approximately similar band combinations. Based on this analysis, three VIs were proposed for this new camera, and their behavior at different stages was evaluated using Leaf Area Index (LAI). Cyan and Orange spectral values were relatively high in the first and last growing seasons, while NIR values increased dramatically in the mid-growing seasons and decreased in the last stage. $VI_{NIR,O,C}$ index showed the best results for mid-growing seasons (correlation with LAI = 0.39 for R5 and R6). $VI_{C,O}$ index showed a high level of details visually (leaves and background) for R4 and R7 than the other indices and correlated highly with LAI (0.48 and -0.5 , respectively). Overall, the study provided new VIs that can be used to effectively analyze Soybean growth dynamics, with different VIs showing reliability over different growing stages.

Keywords: cyan; orange; near infrared; soybean; leaf area index (LAI); vegetation indices



Citation: Vásquez, R.A.R.; Heenkenda, M.K.; Nelson, R.; Segura Serrano, L. Developing a New Vegetation Index Using Cyan, Orange, and Near Infrared Bands to Analyze Soybean Growth Dynamics. *Remote Sens.* **2023**, *15*, 2888. <https://doi.org/10.3390/rs15112888>

Academic Editors: Chung-Te Chang and Junhu Dai

Received: 28 April 2023

Revised: 24 May 2023

Accepted: 30 May 2023

Published: 1 June 2023



Copyright: © 2023 by the authors. Licensee MDPI, Basel, Switzerland. This article is an open access article distributed under the terms and conditions of the Creative Commons Attribution (CC BY) license (<https://creativecommons.org/licenses/by/4.0/>).

1. Introduction

Several natural and anthropogenic factors, such as irrigation, nutrition, sunlight, and temperature, affect vegetation health dynamics [1]. Lack or excess of those variables leads to visible signs on vegetation or their growth dynamics, resulting in reduced yield or poor-quality harvest. According to the precision agronomy concept, good management and fewer resources can deliver better results, improving the crop's health and yield [2]. Usually, farmers use their traditional knowledge, visual greenness observations, and empiric methods to determine plant health, ultimately making management decisions to protect their cultivations. The green color of a plant is an indicator of its level of chlorophyll which absorbs sunlight for the photosynthesis process [3]. Therefore, leaf chlorophyll can be used to estimate leaf photosynthetic capacity and, thus, vegetation health because of its close relationship with leaf nitrogen content that affects vegetation growth dynamics [4,5]. The procedures commonly used to determine leaf chlorophyll are destructive chemical analysis methods that involve the extraction of chlorophyll from leaf matter with organic solvents, followed by a spectrophotometric assay of chlorophyll [6–8]. However, this approach is time-consuming and expensive. Recently, several remote sensing approaches (indirect) were introduced to estimate vegetation health [9]. These remotely sensed methods

are non-destructive, fast, and efficient. Vegetation health or vigor can be indirectly observed by using vegetation indices (VIs) derived from remotely sensed images [10]. Another variable used to measure health is the Leaf Area Index (LAI), the ratio of leaf area to ground area, typically reported as meters per square meter, a commonly used biophysical characteristic of vegetation [11]. It was also determined that LAI could be related to yield, another indicator of vegetation health, following the idea that healthy plants will have greater yield results than unhealthy plants [11].

1.1. Remote Sensing for Assessing Vegetation Health

Remote sensing of vegetation health monitoring provides time, cost-effective, and repeatable recordings and evaluations of status, stress, disturbances, and resource limitations over the short to long term for local and global vegetation monitoring [12,13]. The broad wavelength region of 400–700 nm is described as the most active region for leaf pigments or chlorophyll [14]. Based on the healthy vegetation spectral profile, healthy leaf pigments show higher reflectance values at the electromagnetic spectrum's green and Near Infrared (NIR) regions [15,16]. Additionally, the Red Edge Region is the best remote sensing region descriptor of chlorophyll concentration (680–750 nm) [4].

A widely used remote sensing approach for health monitoring is using Vegetation Indices (VIs) derived from different band combinations to detect vegetation changes over time. Mathematical expressions of VIs can be selected to show how different plant components reflect the amount of electromagnetic energy. Therefore, VIs provides quantitative measures of vegetation health. This approach is time and cost-effective, reliable, and quickly covers large areas. The existing mathematical formulas for VIs were developed considering the healthy vegetation spectral profile and thus provide reasonable measures for vegetation dynamics [17]. Several studies used LAI, which is also a parameter for global and regional models of the biosphere/atmosphere exchange of carbon dioxide and water vapor, light interception, and other leaf functions and processes (photosynthesis) to predict chlorophyll content using remote sensing techniques [4,5,18–20]. For instance, the spatial distribution of mangrove canopy chlorophyll content can be mapped by using laboratory-measured canopy chlorophyll concentrations, LAI, and remotely sensed images [20].

Existing Vegetation Indices

Many of the existing VIs use the NIR and red spectral bands in different mathematical combinations to express quantitative and qualitative features; for example, one of the widely used VIs is the Normalized Difference Vegetation Index (NDVI); this index indicates the structure and greenness of vegetation using NIR and red spectral bands as expressed in Table 1. Carotenoid Reflectance Index 1 (CRI1), which ranges from one to eleven for green vegetation, is commonly used to assess stressed vegetation [21].

Table 1. Selected Vegetation Indices that are approximately equal to the spectral bands used in this study.

Vegetation Index	Mathematical Expression
Difference Vegetation Index (DVI) [22]	$\text{NIR} - \text{Red}$
Ratio Vegetation Index (RVI) [23]	Red/NIR
Normalized Difference Vegetation Index (NDVI) [24]	$(\text{NIR} - \text{Red})/(\text{NIR} + \text{Red})$
Carotenoid Reflectance Index 1 (CRI1) [21]	$1/P_{510} - 1/P_{550}$
Soil Adjusted Vegetation Index (SAVI) [25]	$((\text{NIR} - \text{Red})/((\text{NIR} + \text{Red}) + L)) \times (1 + L)$

In the visible spectral range (approximately 380–700 nm), the blue, green, and red bands are the most used bands. For example, two perpendicular vegetation index (PVI) models were applied, the PVI and PVI6, that yielded significant coefficients of determination (R^2) of 0.522 and 0.659, respectively, with LAI [22]. It is possible to use the visible

spectral range, specifically the green region, to sense the chlorophyll concentration in order to measure the rate of photosynthesis and to monitor plant stress [26].

With the development of technology, new sensors with different spectral band combinations than the traditional blue, green, red, and NIR are being introduced to the market. For instance, Mapir Survey 3W OCN camera is sensitive to the Cyan (480–520 nm), Orange (585–620 nm), and NIR (780–870 nm) [2] (Table 2). According to the OCN camera specifications, the OCN camera is the improved version of the RGN camera, which is sensitive to green (530–570 nm), red (640–680 nm), and NIR (820–880 nm) bands of the electromagnetic spectrum by increasing the contrast within vegetation and reducing soil noise [27,28]. The OCN camera is more sensitive to a relatively wide NIR region than the RGN camera. However, there is no in-depth analysis of spectral profiles of different bands or VIs for OCN camera band combinations as this camera is relatively new. Therefore, this study aimed to develop a new VI for analyzing Soybean plant growth dynamics using the OCN camera, which is sensitive to the electromagnetic spectrum's Cyan, Orange, and NIR bands. The specific objectives are to (1) develop a spectral profile for Soybean's growing stages; (2) compare the performance of different VIs at different growing seasons; (3) validate the performance using Canopy LAI; and (4) propose the best-fitted VI for Cyan, Orange and NIR bands.

Table 2. Bandwidth (nm) for Mapir Survey 3 Wide-angle RGN and OCN cameras.

Mapir Survey 3 (Wide Angle)					
OCN Camera			RGN Camera		
Cyan 460–520	Orange 585–645	NIR 780–870	Green 530–570	Red 640–680	NIR 820–880

2. Materials and Methods

2.1. Data and Study Area

The study was conducted at the Lakehead University Agriculture Research Station (LUARS), Thunder Bay, Ontario, Canada (48.3051°N, 89.3881°W). Several Soybean species were tested on a large area (87 m × 32 m area), and the study selected two locations to set up cameras (Figure 1).

A massive increase in Soybean production and international trade during the past 60 years has been a significant cause of the world's average human life span increasing from 46.6 to 69.3 years during that time period [29]. An increase in dietary protein has been especially beneficial in developing countries where diets have historically been too low in protein [29]. In Canada, Soybean is a highly produced crop, with over 1,260,400 seeded hectares in Ontario [30].

Remote Sensing DataImage acquisition started on 26 July 2022 and finished on 19 September 2022: This study followed the regional reproductive stage identification details and divided the period into four reproductive stages, hereafter denoted as “R4–R7” [31,32]; Reproductive Stage 8 (R8) was the harvesting stage.

The study used two Mapir Survey 3W aerial cameras [33]. One is sensitive to Red (660 nm), Green (550 nm), and NIR (850 nm) bands (hereafter denoted as “RGN camera”), and the other is sensitive to Cyan (490 nm), Orange (615 nm), and NIR (808 nm) bands (hereafter denoted as “OCN camera”); Table 2 explains the spectral range of these cameras. Noticeably, the NIR regions of the cameras are different (Table 2). Two Soybean plots were selected for analysis based on their plant density. Station 01 had sparsely distributed Soybean plants, and two cameras (OCN and RGN) were set up at a 90° angle (looking straight down) (Figure 2). Station 02 had dense Soybean plants and arranged two cameras at a 90° angle (OCN camera) and a 45° angle (RGN camera) (Figure 2). Images were captured every 30 min daily from 7.00 a.m. to 5.30 p.m. during the season. Images were downloaded once a month and sorted into the different reproductive stages and times of the day morning (7:00 a.m. to 11:00 a.m.), midday (11:00 a.m. to 2:00 p.m.), and

afternoon (2:00 p.m. to 5:00 p.m.). Then, they were calibrated (converted DN values to spectral reflectance values) using the MAPIR Camera Control (MCC) Software version 20221111 [34] for further analysis using R Studio [35].



Figure 1. A map of the Lakehead University Agricultural Research Station. The Soybean plot and the camera stations were indicated using a black polygon outline and blue/red points, respectively.

2.2. Spectral Signatures

To derive spectral profiles for each stage using an OCN camera, approximately 30 midday images were selected for each stage (R4–R7); a random set of points were selected inside Soybean leaves and extracted corresponding spectral reflectance values for each band. There were approximately 1000 data points for each stage. Exploratory Data Analysis (EDA) was done based on scatter plots (index plots), box plots, histograms, and Q-Q plots. Based on EDA, outliers were removed, and a set of spectral reflectance values for each stage was prepared (1000 points per each stage). The spectral values were plotted against each wavelength, and the mean spectral profiles were extracted for each stage (R4–R7).

2.3. Vegetation Indices

To date, no unified mathematical expression defines all VIs due to the complexity of different light spectra combinations, instrumentation, platforms, and spectral and spatial resolutions used [10]. Table 1 shows selected VIs that use approximately the same spectral bands as one of the cameras used for this study.

To develop the new VI, several existing band combinations (mathematical expressions) were initially tested (Table 3). A set of random points were selected inside Soybean leaves, and corresponding VI values were extracted. This was repeated for all images and stages. The correlation between index values and spectral reflectance values was analyzed. Based on these results, three options were proposed as new VIs for OCN cameras (Table 4).



Figure 2. Camera Station Setups at different angles; cameras were operated using the power generated from a battery and a solar panel at each station. Raspberry Pi micro-computers were used to automate the image acquisition process.

Table 3. Tested Vegetation Indices based on existing Vegetation Indices.

Original Vegetation Index	Symbology	Proposed Vegetation Index
Difference Vegetation Index (DVI)	dvi_on	NIR – Orange
Ratio Vegetation Index (RVI)	sr_on	Orange/NIR
Ratio Vegetation Index (RVI)	sr_cn	Cyan/NIR
Normalized Difference Vegetation Index (NDVI)	ndvi_on	$(\text{NIR} - \text{Orange}) / (\text{NIR} + \text{Orange})$
Adjusted Vegetation Index (SAVI)	savi_on	$(1.5 \times (\text{NIR} - \text{Orange})) / (\text{NIR} + \text{Orange} + 0.5)$

Table 4. New Vegetation Indices.

Symbology	Mathematical Expression
$VI_{\text{NIR},\text{O},\text{C}}$	$\left(\frac{\text{NIR} - \text{Orange}}{\text{NIR} + \text{Orange}} \right) \times \left(\frac{\text{NIR}}{\text{Cyan}} \right)$
$VI_{\text{NIR},\text{O},\text{O}}$	$\left(\frac{\text{NIR} - \text{Orange}}{\text{NIR} + \text{Orange}} \right) \times \left(\frac{\text{NIR}}{\text{Orange}} \right)$
$VI_{\text{C},\text{O}}$	$\left(\frac{\text{Cyan}}{\text{Orange}} \right)$

2.4. Leaf Area Index

LAI was calculated using an indirect method introduced in a study conducted in the North American region (Nebraska), which indicated successful results [36]. Gaso et al. [37] also effectively used LAI in their study of Soybean yield variability. We selected Equation (1) with a Root Mean Squared Error (RMSE) of 0.48 and a coefficient of determination (R²) of 0.90 to calculate the LAI of our Soybean plants.

$$\text{LAI} = \log_{0.37} \left(\text{NDVI}^{-0.526} - 1.03 \right) \quad (1)$$

NDVI was calculated using images from the RGN camera. Once LAI was calculated, values were extracted for the same set of random points (as used earlier for VIs). EDA was performed to remove outliers and understand the data distribution.

2.5. Proposed Indices and Their Validation

The new VIs were calculated for each stage; corresponding values were extracted for the same set of random points. EDA was completed, and outliers were removed. Since data were not normally distributed at all stages, the Kruskal-Wallis test [38] was used to determine if there were significant differences between the new VIs and LAI. After that, Pearson Correlation Coefficient (r) was calculated between the new VIs and LAI to evaluate how representative they are at different stages [39].

3. Results

3.1. Spectral Profiles

According to Figure 3 (R4 stage), there were outliers in the Cyan and Orange bands. The index plots are scatterplots with the spectral value of the points (y -axis) appearing from left to right in the order they are available in the data file. So the scatter plot shows spectral values from left to right according to each stage's ascending order of date and time. However, data were not trended, and the degree of scatter was consistent from left to right (see scatter plots). NIR values were approximately normally distributed without outliers. The theoretical quantile plots were used to determine how these points deviated from a theoretical normal distribution and visually assess whether the difference was significant. Once outliers were removed, these deviations were insignificant for this stage. The spectral profiles are shown in the upper right graph. Grey lines represent data points, and the black line represents the average spectral profile for the R4 stage. The Orange band value was slightly lower than NIR values and higher than the Cyan value. However, NIR values were seen increasing at later dates. Figure 4 shows the R5 stage. All bands had outliers, and the NIR scatter plot showed a positive trend (data ranging from 0.6 to 1). Data points significantly deviated from theoretical normality (theoretical quantile plots and histograms). Once outliers were removed, the average spectral profile indicated dramatically increased NIR and low Cyan and Orange values. Almost the same spectral behaviors were evident in the R6 stage (Figure 5). The average spectral profile of R6 was similar to R5. According to Figure 6, the data for the R7 stage had few outliers and had an average spectral profile more similar to R4 than either R5 or R6, with a NIR value range of 0.2 to 0.8.

Table 5 shows the mean and Standard Deviation (SD) of band values at each stage. The Orange band got higher mean values in R4 (0.28) and R7 (0.24) stages with lower mean values in R5 (0.13) and R6 (0.09). NIR values were changed from 0.38, 0.91, and 0.88 to 0.42 for R4–R7, respectively (Table 5).

Table 5. OCN bands Mean and Standard Deviation among Reproductive Stages.

Band	R4		R5		R6		R7	
	Mean	SD	Mean	SD	Mean	SD	Mean	SD
Cyan	0.08	0.06	0.08	0.04	0.06	0.03	0.04	0.04
Orange	0.28	0.09	0.13	0.05	0.09	0.04	0.24	0.14
NIR	0.38	0.22	0.91	0.12	0.88	0.13	0.42	0.20

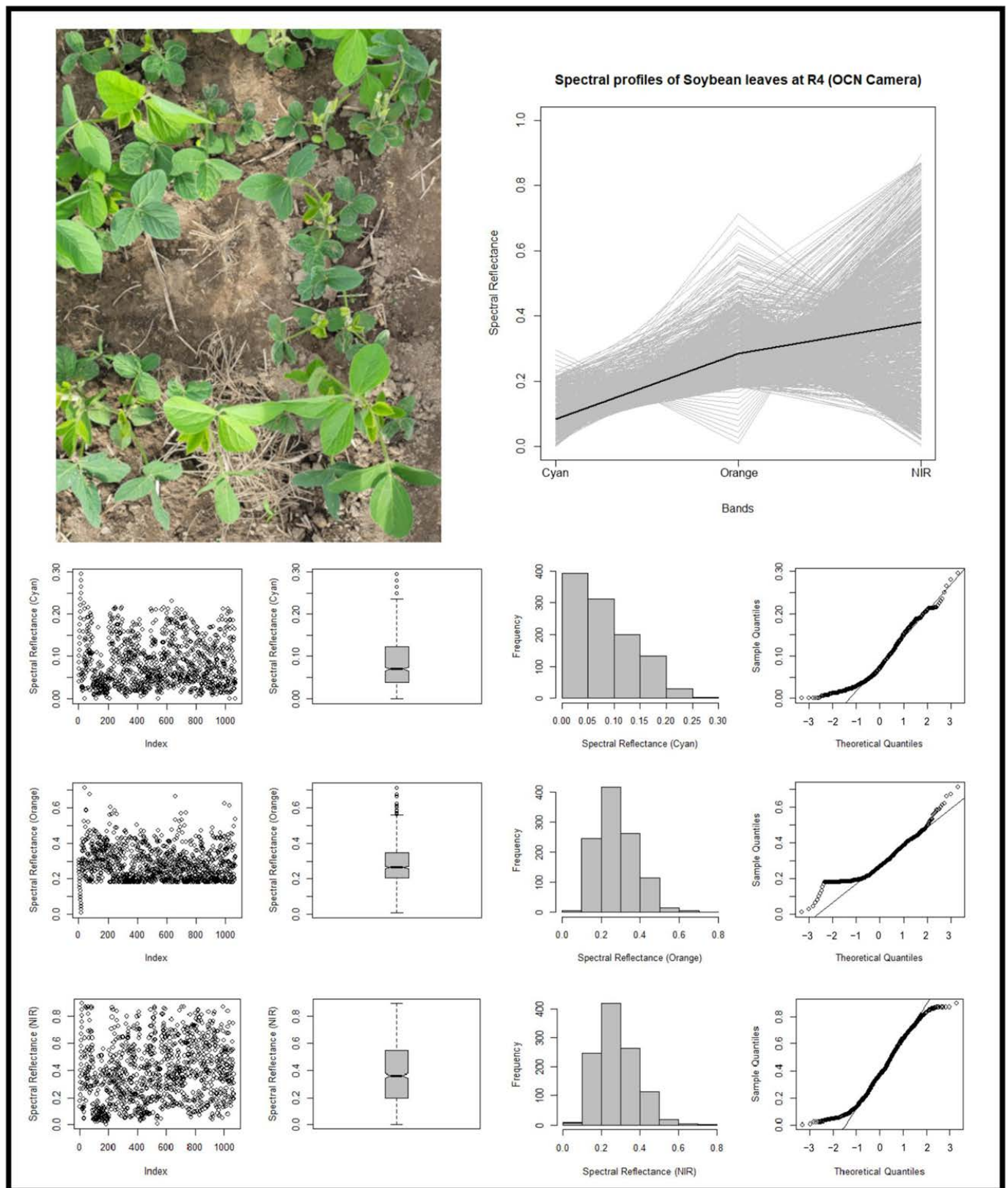


Figure 3. The average OCN spectral profile and Exploratory Data Analysis for the R4 stage. The upper left shows an example of the R4 stage. The upper right is the spectral profiles of 1000 points from the OCN camera (grey lines) and the average spectral profile of the reproductive stage (black line). The lower part of the image includes exploratory data analysis results for each band (Scatter plot (index plot); box plot; histogram, and theoretical quantiles, respectively).

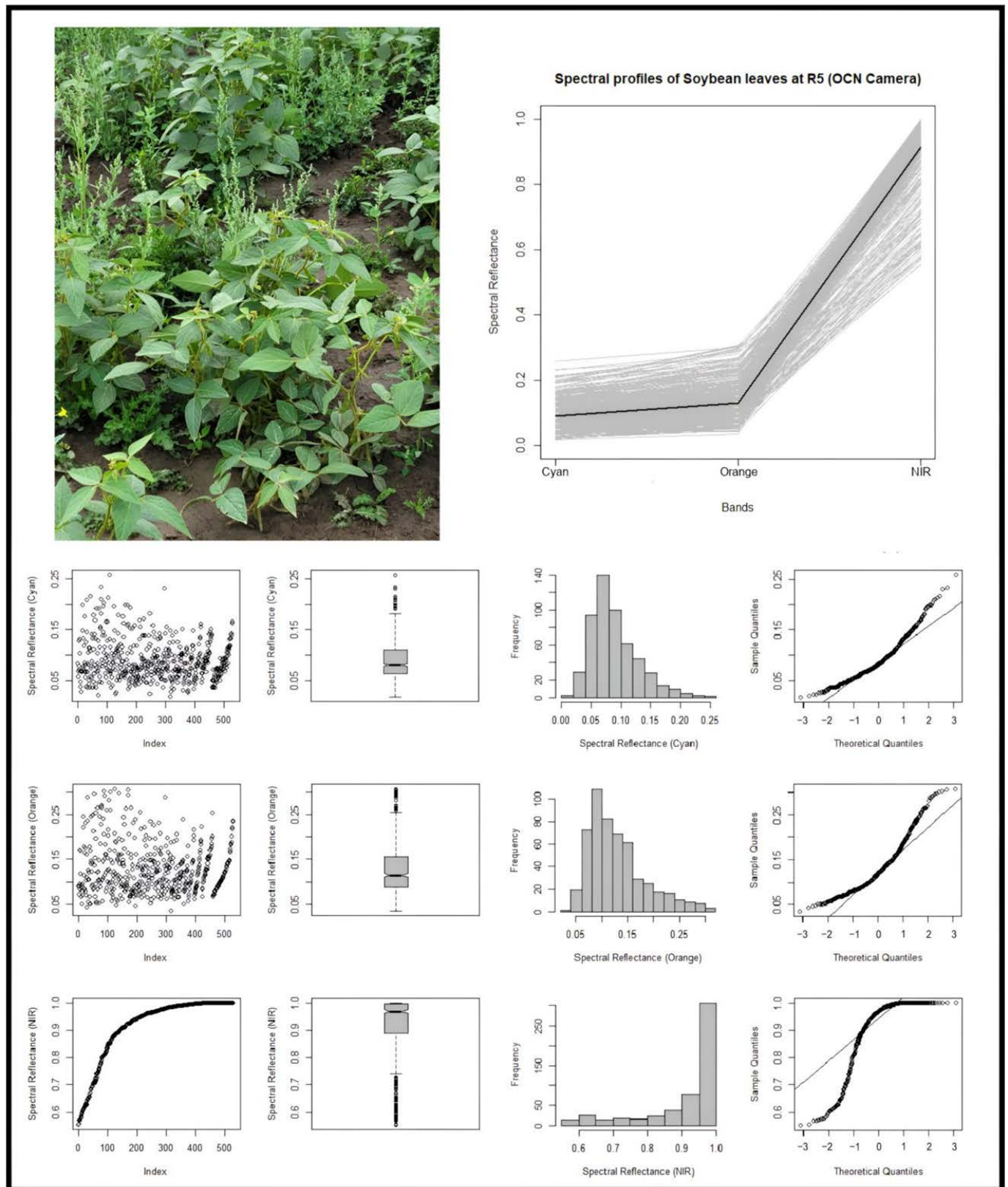


Figure 4. The average OCN spectral profile and Exploratory Data Analysis for the R5 stage. The upper left shows an example of the R5 stage. The upper right is the spectral profiles of 1000 points from the OCN camera (grey lines) and the average spectral profile of the reproductive stage (black line). The lower part of the image includes exploratory data analysis results for each band (Scatter plot (index plot); box plot; histogram, and theoretical quantiles, respectively).

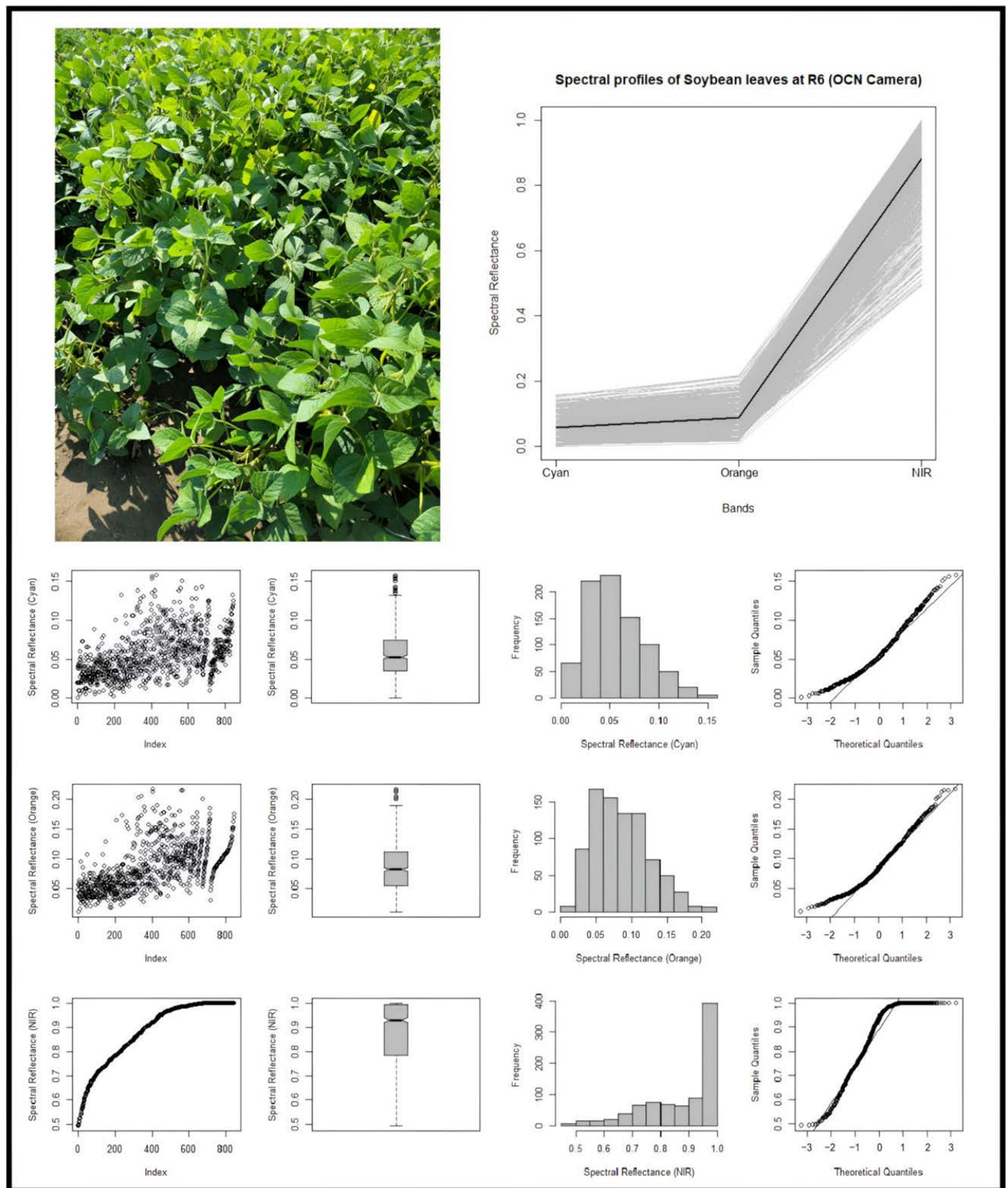


Figure 5. The average OCN spectral profile and Exploratory Data Analysis for the R6 stage. The upper left shows an example of the R6 stage. The upper right is the spectral profiles of 1000 points from the OCN camera (grey lines) and the average spectral profile of the reproductive stage (black line). The lower part of the image includes exploratory data analysis results for each band (Scatter plot (index plot); box plot; histogram, and theoretical quantiles, respectively).

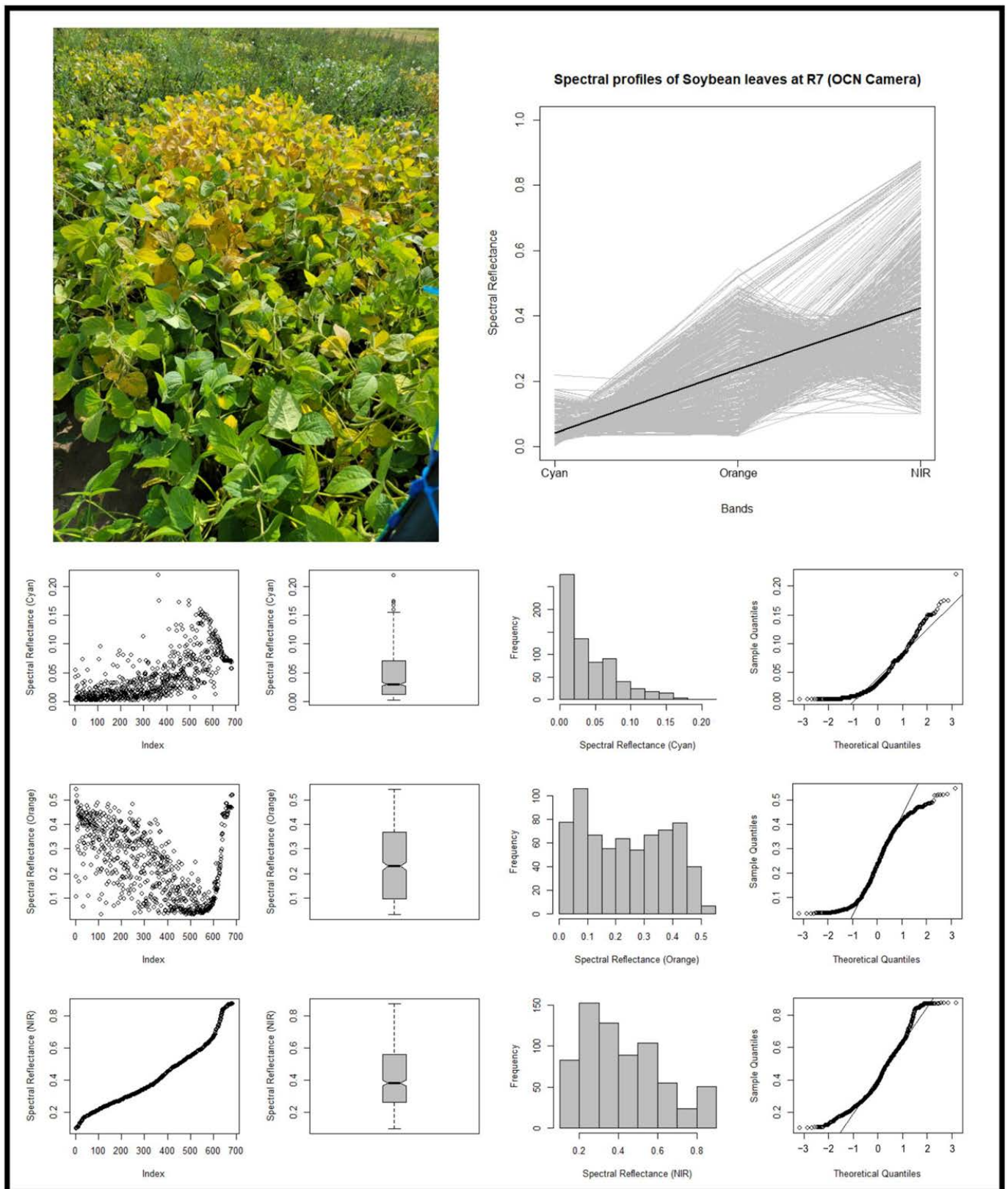


Figure 6. The average OCN spectral profile and Exploratory Data Analysis for the R7 stage. The upper left shows an example of the R7 stage. The upper right is the spectral profiles of 1000 points from the OCN camera (grey lines) and the average spectral profile of the reproductive stage (black line). The lower part of the image includes exploratory data analysis results for each band (Scatter plot (index plot); box plot; histogram, and theoretical quantiles, respectively).

3.2. Proposed Indices

3.2.1. Correlation between Different Spectral Bands and VIs (OCN Camera)

Figures 7–10 show the correlation between different vegetation indices and spectral bands of the OCN camera. Within the bands themselves, the scatterplots didn't show linear correlations. However, in R5 and R6 stages, Cyan and Orange bands showed a statistically significant positive linear correlation (0.973) (Figures 8 and 9). There is a non-linear, moderate negative correlation (−0.387) in R4 and R7. In the R4 stage, there is a non-linear, negative correlation between Orange and NIR bands (−0.206) (Figure 7) and a strong positive relation between Cyan and NIR bands. Additionally, the index “ndvi_on” presents statistically significant (negative) correlations between indices “sr_cn” and “sr_on”. These patterns are almost similar at the R7 stage (Figure 10). In R5 and R6 stages, there is a high correlation between “ndvi_on” and the indices “sr_cn” and “sr_on” correlation (Figures 8 and 9).

Referring to Figures 7–10, a relationship between different bands or two indices with a high degree of correlation can be explained with the following generic equation:

$$VI_1 \propto VI_2 \tag{2}$$

where $VI_{1\&2}$ vegetation indices are derived from the OCN camera using existing mathematical formulas.

According to Figures 7–10 and Equation (2), there were no strong linear relationships between different bands or band combinations. Hence, the mathematical expressions proposed in Table 4 were polynomial (quadratic) equations. For example, Figure 7 shows quadratic relation with NIR for the other two bands. For example, there was a statistically negative relation ($r = -0.991$) between ndvi_on and sr_on, and it was the basis for the proposed $VI_{NIR,O,C}$ index.

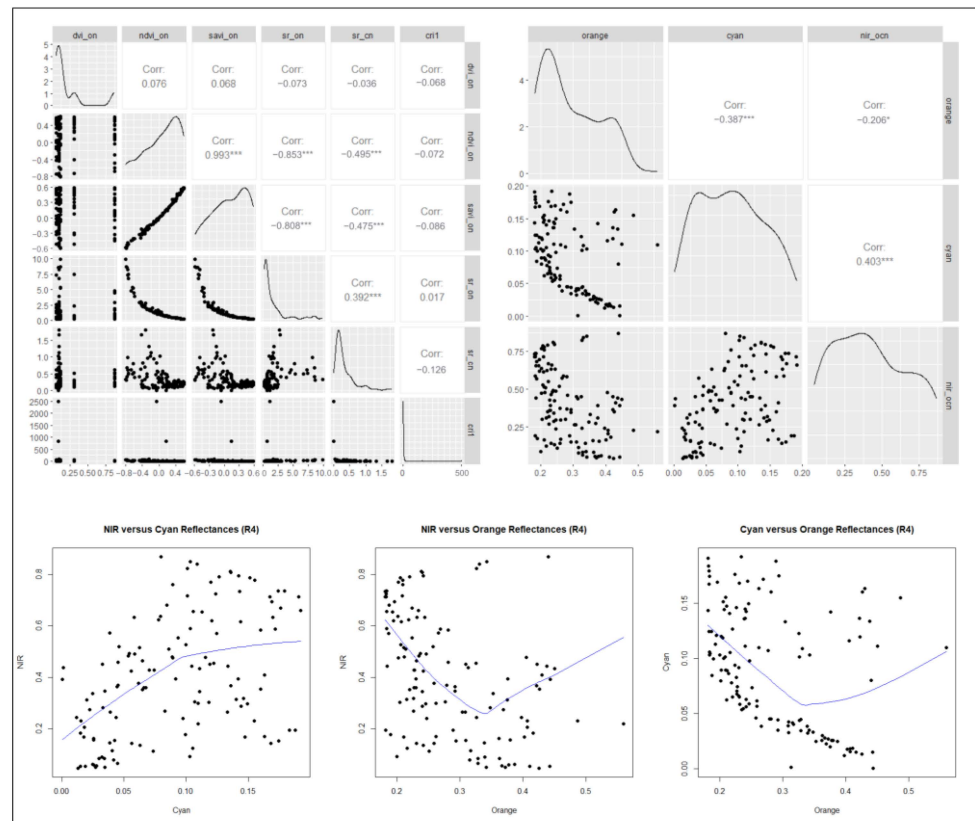


Figure 7. Correlations between different combinations of spectral bands (Cyan, Orange, and Near-Infrared) and Vegetation Indices derived from the OCN camera at the R4 stage. Symbol * represents the level of statistical significance of correlation. Points are part of scatterplots with a fitted line (blue).

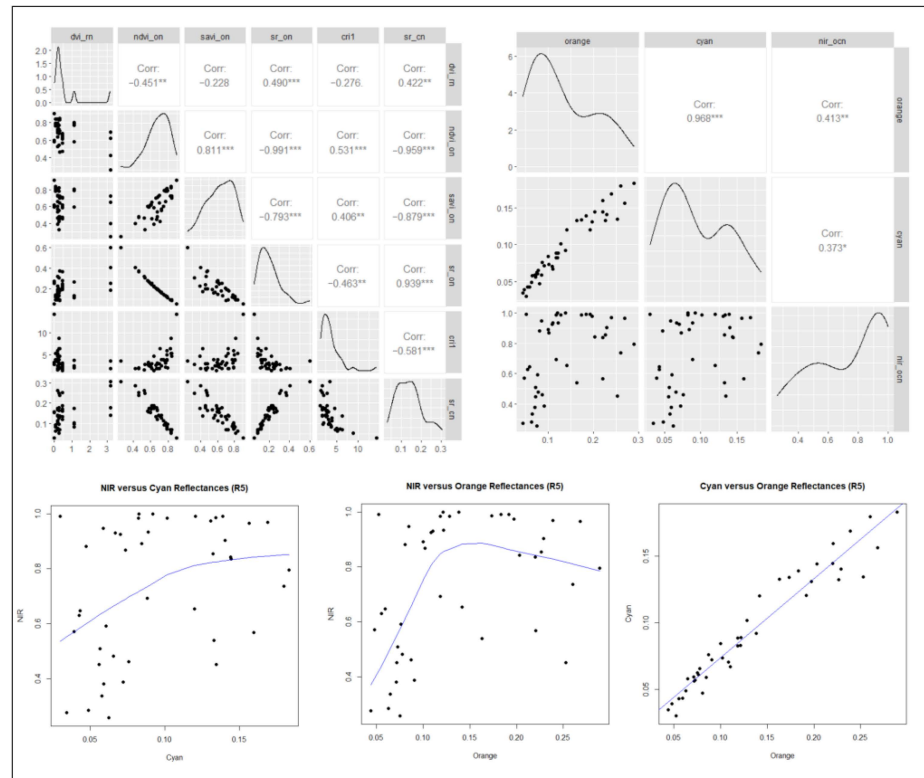


Figure 8. Correlations between different combinations of spectral bands (Cyan, Orange, and Near Infrared) and Vegetation Indices derived from the OCN camera at the R5 stage. Symbol * represents the level of statistical significance of correlation. Points are part of scatterplots with a fitted line (blue).

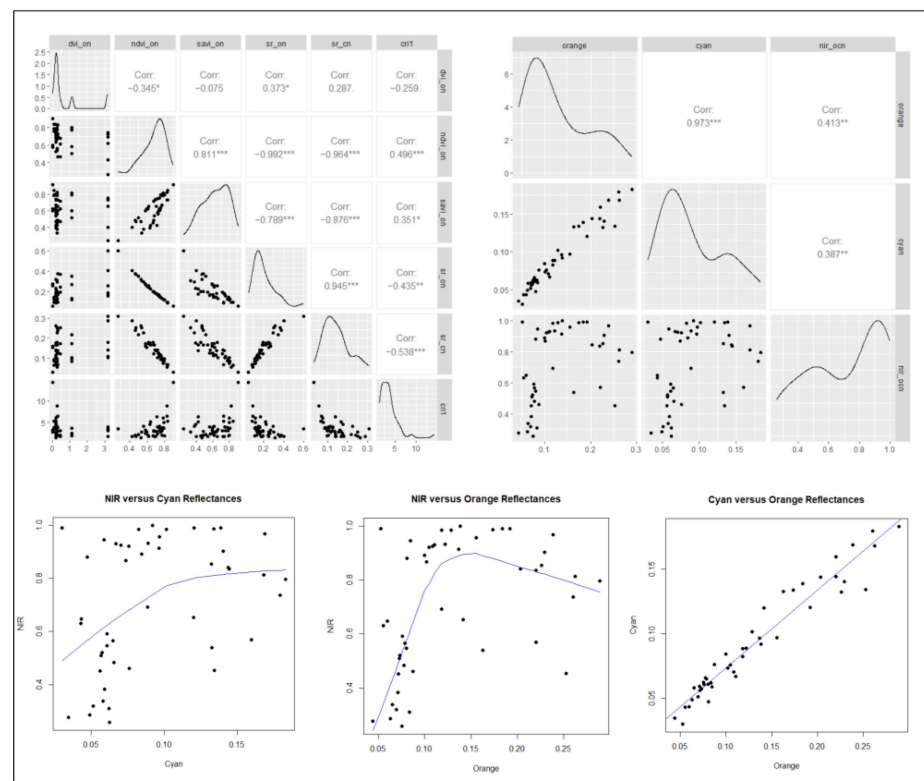


Figure 9. Correlations between different combinations of spectral bands (Cyan, Orange, and Near Infrared) and Vegetation Indices derived from OCN camera at the R6 stage. Symbol * represents the level of statistical significance of correlation. Points are part of scatterplots with a fitted line (blue).

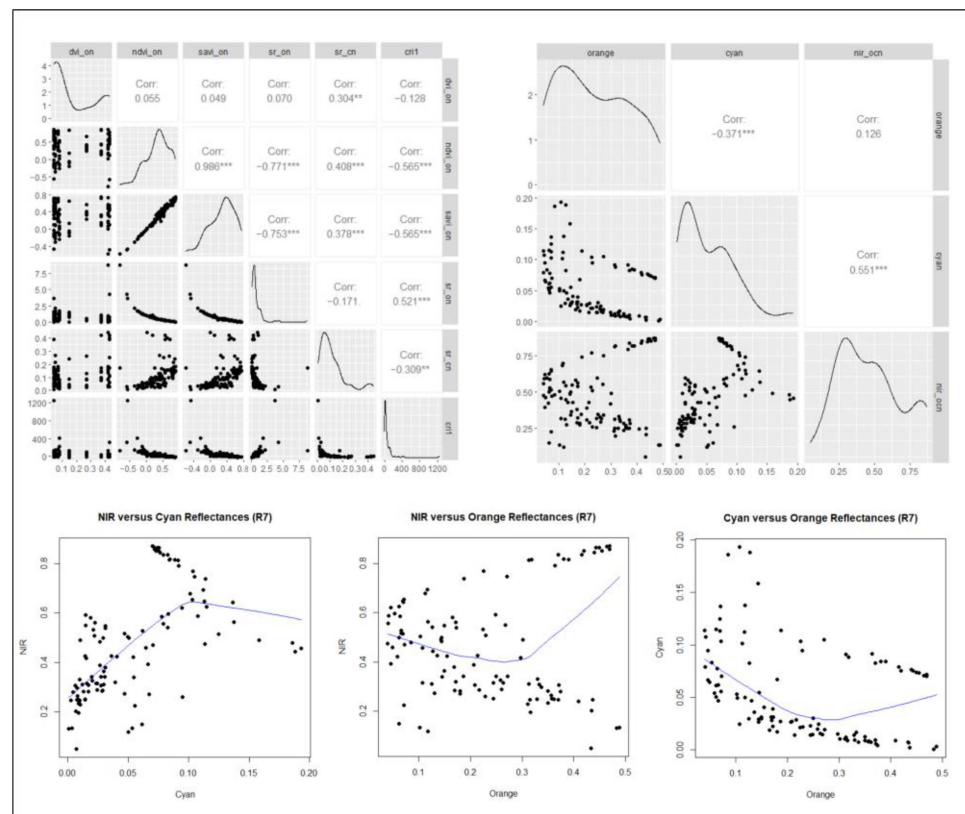


Figure 10. Correlations between different combinations of spectral bands (Cyan, Orange, and Near Infrared) and Vegetation Indices derived from OCN camera at the R7 stage. Symbol * represents the level of statistical significance of correlation. Points are part of scatterplots with a fitted line (blue).

3.2.2. Correlation between LAI and New VIs

The New VIs were tested over the growing season and assessed the reliability of them based on the LAI of Soybean plants. The Kruskal Wallis test results for LAI and different indices values were not statistically significant at the 95% confidence level (p -value > 0.05), indicating no significant difference between LAI values and new VIs at each stage.

The correlation between the new VIs and LAI is summarized in Table 6. $VI_{NIR,O,C}$ showed a higher correlation for middle stages (R5 and R6), slightly better than $VI_{NIR,O,O}$. The index: $VI_{C,O}$ showed a moderate positive correlation for R4 and a moderate negative correlation for R7 (Table 6). Figure 11 shows examples of the new VIs for each stage. Although R5 and R6 had a linear correlation between Cyan and Orange bands, the $VI_{C,O}$ didn't differentiate Soybean leaves and the background properly (Figure 11, rows 2 and 3). This is also evident in the correlation between LAI and indices (Table 6). However, $VI_{C,O}$ showed a visually high level of details (leaves and background) for R4 and R7 than the other indices. $VI_{NIR,O,C}$ in R5 and R6 showed the same, where more details can be appreciated within the leaves and a clear demarcation between leaves and the background.

Table 6. Pearson Correlation Coefficient (r) results between the New Vegetation Indexes and LAI for each stage.

VI	Stage			
	R4	R5	R6	R7
$VI_{NIR,O,C}$	0.44	0.39	0.39	0.2
$VI_{NIR,O,O}$	0.29	0.37	0.38	−0.3
$VI_{C,O}$	0.48	−0.27	0.28	−0.5

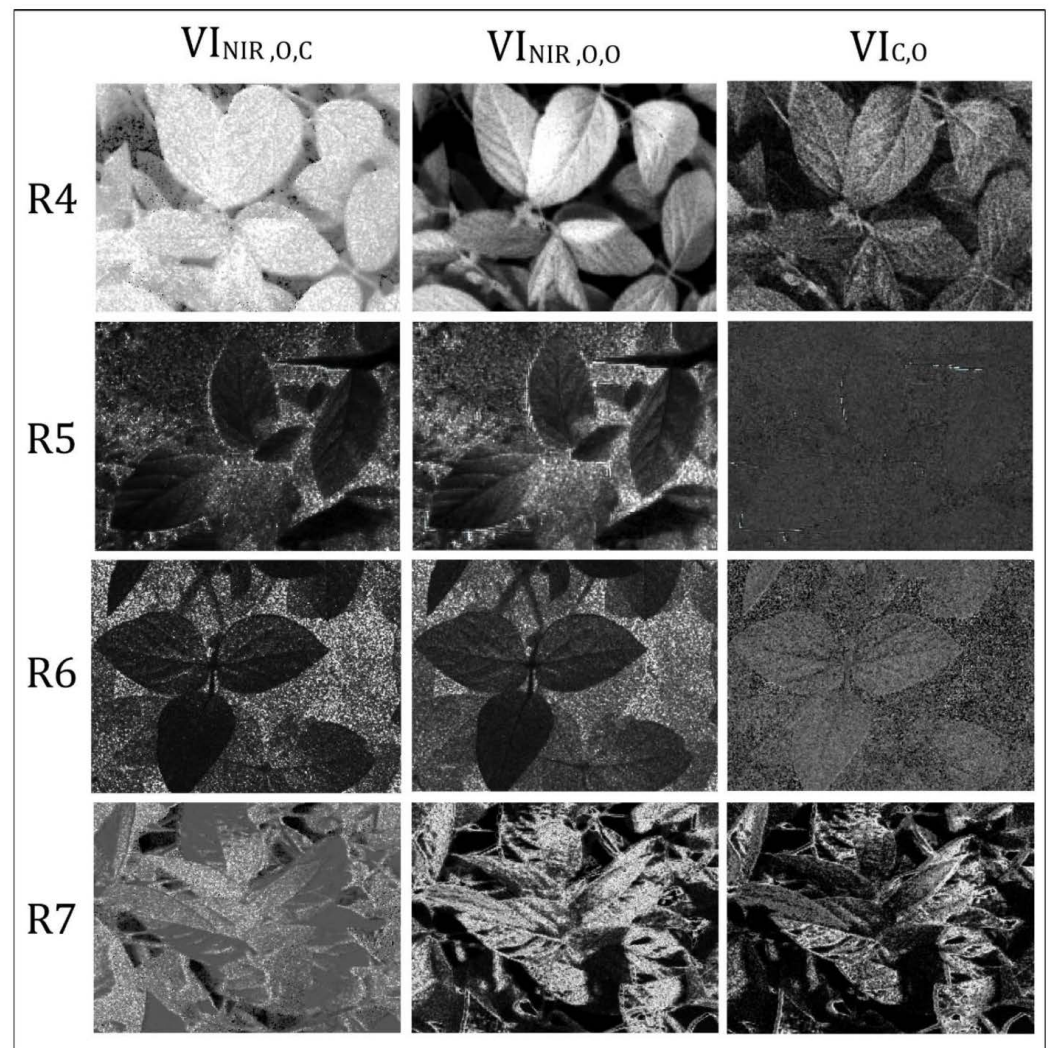


Figure 11. New Vegetation Indices were shown in different reproductive stages. $VI_{C,O}$ shows visually appealing results for R4 and R7, while $VI_{NIR,O,C}$ got better results for R5 and R6.

4. Discussion

Photographs of each growing stage in Figures 3–6 show Soybean maturity levels. For example, R4 had pre-matured plants (early stage), and R7 was in the late season showing yellowish plants. It is also important to note that images from R4 and R7 stages, where plants were sparsely distributed, have soil in the background which must be separated from the leaf area in the analysis. In R5 and R6, plants were fully grown, and no soil was visible in the camera's field of view.

4.1. Spectral Profiles

According to the data analysis, it can be confirmed that the generated spectral profiles followed the standard healthy vegetation spectral profile pattern. For example, the average Cyan values were 0.08 (R4 and R5), changed from 0.08 to 0.06 (R5 to R6), and further reduced to 0.04 in R7 (Table 5). In contrast, Orange spectral values were reduced from R4 to R5 and further in R6 and then increased from R6 to R7. When plants are maturing, chlorophyll and carotenoid concentration will change, and thus the absorption near the red region varies [1–3]. Results showed a low NIR reflectance for R4 and R7, stages where leaf pigments (leaf chlorophyll and carotenoids) are expected to be lower than in other stages. High NIR reflectance in the middle stages (R5–R6) indicates fully grown Soybean with high leaf chlorophyll concentrations [1–3]. Hence, these results coincided with the already

developed healthy vegetation spectral profile [15,16]. Although Kokaly et al. [14] stated the wavelength region of 400–700 nm is sensitive to changes in leaf pigments and thus the leaf chlorophyll content, the NIR wavelength region of the OCN camera (780–870 nm) is outside the specified ideal range. This study also indicated meaningful variations of NIR within growing stages. The NIR spectral values in the mid and later stages showed a positive trend during EDA until the latter part of the R7 stage, which indicates a negative trend. A study comparing actual leaf chlorophyll concentration and spectral values is recommended.

4.2. Proposed Indices

No linear relations existed between individual bands except Cyan and Orange bands in the mid-seasons (R5 and R6). This can be explained in terms of chlorophyll and carotenoid concentration variations over the growing season and their effect on sunlight absorption and reflection. For example, when plants mature, chlorophyll (greenness) increases and thus absorption in the near the red region and increasing reflectance in green (near Cyan) [15,16,40]. On the other hand, as specified in Gutman et al. [41] and other studies, NIR and red didn't show a linear relation. As noted, R5 and R6 had similar patterns as did R4 and R7. A different level of exposure to the soil background might contribute here. The existing vegetation indices derived using the OCN camera, according to Table 3, were based on linear relations of different band combinations. Hence, the new indices were derived by analyzing the correlation between those indices. For example, "ndvi_on" and "sr_cn" had statistically significant high negative relation (-0.9), and it was the basis for $VI_{NIR,O,C}$ index.

Visual analysis of images derived from the new indices illustrates different levels of detail in the vegetation depending on the index and growth stage (Figure 11). This is compatible with the correlation coefficients obtained in Table 6. For instance, $VI_{NIR,O,C}$ showed good results for R5 and R6, which is clearly shown in Figure 11. Since there was a similar correlation between Cyan and Orange bands in R4 and R7, the new index: $VI_{C,O}$ showed good results. Although there was a strong linear relationship between Cyan and Orange at R5 and R6 stages, the ratio of these two bands didn't differentiate Soybean leaves well. That indicates their low reflectance values in these stages. Once these two bands were combined with the NIR band using a polynomial equation, the results were acceptable (Table 6).

LAI is a key biophysical variable used to measure crop growth and productivity [11]. Hence, we used LAI to assess whether the details of the Soybean plot represented by the proposed indices were the same as the distribution of LAI. The statistical analysis Kruskal-Wallis test didn't show a significant difference between index values and LAI.

Due to time limitations, we were not able to test the spectral variations over small time spans, so the data, which was collected multiple times each day were, aggregated into growing stages. It would be beneficial to analyze the same set of data as time series to see the spectral variations over time. In the future, it would recommend comparing the vegetation indices to the leaf chlorophyll content to assess the performance of the proposed indices. Additionally, testing the proposed indices over another growing season or including a lab chemical analysis, perhaps for nitrogen variations, would represent an important accuracy assessment.

4.3. Practical Applications of Results

The study developed spectral profiles and VIs for different Soybean growth stages. For example, in a practical situation, field spectral profiles can be compared with this study's generated spectral profile and make informed decisions regarding the Soybean growth patterns, even at different reproductive stages. The proposed VIs are useful, especially in analyzing growth dynamics over a large area; for instance, this camera can be attached to a Remotely Piloted Aircraft System (RPAS or drone), capture images and calculate the proposed VIs for large Soybean fields to assess the growth patterns over time.

5. Conclusions

Using remote sensing technology, we developed new vegetation indices (VIs) from the Mapir Survey 3W OCN camera that includes the Cyan, Orange, and NIR bands from the electromagnetic spectrum on two adjustable stations attached to Raspberry Pi units and solar panels. This approach provides a cost-effective and efficient method for precise crop management. We analyzed spectral information from four Soybean reproductive stages (R4–R7) at LUARS, conducted EDA, and removed outliers. We then created and analyzed spectral profiles for each stage.

Our analysis revealed that the spectral profiles obtained for each stage were consistent with what is expected from healthy vegetation spectral profile studies. The Cyan values ranged from 0.08 to 0.09 (R4 to R5) and 0.05 to 0.09 (R5 to R6) and remained the same in R7. The Orange spectral values decreased from R4 to R5 and increased from R6 to R7, while the NIR values were higher in the middle stages and lower in R4 and R7 stages, where chlorophyll is expected to be in a lower concentration. We tested correlations between each spectral band at different stages and found a positive linear relation between Cyan and Orange reflectance in R5 and R6 stages, while all other combinations were non-linear.

We then tested various existing VIs that utilized similar band combinations and found that combining Cyan and Orange with NIR in a polynomial equation delivered strong correlations. Based on these findings, we proposed three VIs: $VI_{NIR,O,C}$, $VI_{NIR,O,O}$, and $VI_{C,O}$. We correlated these VIs against LAI values and obtained results of 0.39 for R4 and R5, 0.48 for R6, and -0.5 for R7 (Table 6). Our analysis suggests that the best-fitted VI for middle stages is $VI_{NIR,O,C} = ((NIR - Orange)/(NIR + Orange)) \times (NIR/Cyan)$, while the best-fitted VI for R4 and R7 is $VI_{O,c} = Cyan/Orange$.

Due to time limitations, we could not test the spectral variations over small periods. Therefore, the data, which was collected multiple times each day, were aggregated into growing stages. Analyzing the same data set as time series would be beneficial to appreciate the spectral variations over time. It is also recommended to compare the vegetation indices with the leaf chlorophyll content to assess the performance of the proposed indices. For further research, it is advisable to conduct testing in another growing season and perform laboratory chemical analyses such as nitrogen content.

In conclusion, our study demonstrates the utility of remote sensing technology in developing a new VI for Soybean crop management. Our findings provide insights into the spectral profiles of Soybeans at different reproductive stages and in different wavelengths, offering new approaches for optimizing crop management.

Author Contributions: Conceptualization, R.A.R.V., M.K.H. and L.S.S.; methodology, R.A.R.V. and M.K.H.; field set up and data collection, R.N., M.K.H. and R.A.R.V.; software, R.A.R.V. and M.K.H.; analysis and validation, R.A.R.V., M.K.H. and L.S.S.; writing—original draft preparation, R.A.R.V.; writing—review and editing, M.K.H., R.N. and R.A.R.V.; project administration, M.K.H., R.N. and R.A.R.V.; funding acquisition, M.K.H. All authors have read and agreed to the published version of the manuscript.

Funding: This research was funded by Agri Risk Initiatives Program, Agriculture and Agri-Food Canada, Microgrant number ARI-IAR-MG-23.

Data Availability Statement: Data are available through a request to the corresponding author.

Acknowledgments: We would like to express our sincere gratitude to Tarlok Singh Sahota, the Director, Lakehead Agriculture Research Station, and Jason Freeburn, Geomatics Technician, Lakehead University, for their valuable advice and technical assistance. Finally, we extend our thanks to our colleagues who provided feedback and support during the development of this project.

Conflicts of Interest: The authors declare no conflict of interest.

References

1. Oregon State University. Environmental Factors Affecting Plant Growth. OSU Extension Service. 2022. Available online: <https://extension.oregonstate.edu/gardening/techniques/environmental-factors-affecting-plant-growth#> (accessed on 6 September 2022).
2. Hemathilake, D.; Gunathilake, D. High-productive agricultural technologies to fulfill future food demands: Hydroponics, aquaponics, and precision/smart agriculture. *Futur. Foods* **2022**, 555–567. [[CrossRef](#)]
3. Roca, M.; Chen, K.; Pérez-Gálvez, A. Chlorophylls. In *Handbook on Natural Pigments in Food and Beverages, Industrial Applications for Improving Food Color*; Woodhead Publishing: Cambridge, UK, 2016; pp. 125–158. [[CrossRef](#)]
4. Filella, I.; Penuelas, J. The red edge position and shape as indicators of plant chlorophyll content, biomass and hydric status. *Int. J. Remote Sens.* **1994**, 15, 1459–1470. [[CrossRef](#)]
5. Houborg, R.; McCabe, M.; Cescatti, A.; Gao, F.; Schull, M.; Gitelson, A. Joint leaf chlorophyll content and leaf area index retrieval from Landsat data using a regularized model inversion system (REGFLEC). *Remote Sens. Environ.* **2015**, 159, 203–221. [[CrossRef](#)]
6. Wellburn, A.R.; Lichtenthaler, H. Formulae and Program to Determine Total Carotenoids and Chlorophylls A and B of Leaf Extracts in Different Solvents. In *Advances in Photosynthesis Research*; Springer: Berlin/Heidelberg, Germany, 1984; pp. 9–12. ISBN 978-94-017-6368-4.
7. Hiscox, J.D.; Israelstam, G.F. Erratum: A method for the extraction of chlorophyll from leaf tissue without maceration. *Can. J. Bot.* **1980**, 58, 403. [[CrossRef](#)]
8. Arnon, D.I. Copper enzymes in isolated chloroplasts. Polyphenoloxidase in *Beta vulgaris*. *Plant Physiol.* **1949**, 24, 1–15. [[CrossRef](#)]
9. Lausch, A.; Bastian, O.; Klotz, S.; Leitão, P.J.; Jung, A.; Rocchini, D.; Schaepman, M.E.; Skidmore, A.K.; Tischendorf, L.; Knapp, S. Understanding and assessing vegetation health by in situ species and remote-sensing approaches. *Methods Ecol. Evol.* **2018**, 9, 1799–1809. [[CrossRef](#)]
10. Xue, J.; Su, B. Significant remote sensing vegetation indices: A review of developments and applications. *J. Sens.* **2017**, 2017, 1353691. [[CrossRef](#)]
11. Watson, D.J. Comparative Physiological Studies on the Growth of Field Crops: I. Variation in Net Assimilation Rate and Leaf Area between Species and Varieties, and within and between Years. *Ann. Bot.* **1947**, 11, 41–76. [[CrossRef](#)]
12. Skidmore, A.; Pettorelli, N. Agree on biodiversity metrics to track from space. *Nature* **2015**, 523, 5–7. [[CrossRef](#)]
13. Turner, W. Sensing biodiversity. *Science* **2014**, 346, 301–302. [[CrossRef](#)]
14. Kokaly, R.F.; Asner, G.P.; Ollinger, S.V.; Martin, M.E.; Wessman, C.A. Characterizing canopy biochemistry from imaging spectroscopy and its application to ecosystem studies. *Remote Sens. Environ.* **2009**, 113, S78–S91. [[CrossRef](#)]
15. Huete, A.R. *Remote Sensing for Environmental Monitoring*; Academic Press: Cambridge, MA, USA, 2004; pp. 183–206. ISBN 9780120644773. [[CrossRef](#)]
16. Acker, J.; Williams, R.; Chiu, L.; Ardanuy, P.; Miller, S.; Schueler, C.; Vachon, P.W.; Manore, M. Remote Sensing from Satellites. In *Reference Module in Earth Systems and Environmental Sciences*; Elsevier: Amsterdam, The Netherlands, 2014; pp. 161–202. [[CrossRef](#)]
17. Roerink, G.; Menenti, M.; Soepboer, W.; Su, Z. Assessment of climate impact on vegetation dynamics by using remote sensing. *Phys. Chem. Earth Parts A/B/C* **2003**, 28, 103–109. [[CrossRef](#)]
18. Liang, S.; Wang, D.; Tao, X.; Cheng, J.; Yao, Y.; Zhang, X.; He, T. Methodologies for Integrating Multiple High-Level Remotely Sensed Land Products. In *Comprehensive Remote Sensing*; Liang, S., Ed.; Elsevier: Amsterdam, The Netherlands, 2018; pp. 278–317. [[CrossRef](#)]
19. Shunlin, L.; Jindi, W. Estimate of vegetation production of terrestrial ecosystem. In *Advanced Remote Sensing*, 2nd ed.; Academic Press: Cambridge, MA, USA, 2020; pp. 581–620. [[CrossRef](#)]
20. Heenkenda, M.K.; Joyce, K.E.; Maier, S.W.; de Bruin, S. Quantifying mangrove chlorophyll from high spatial resolution imagery. *ISPRS J. Photogramm. Remote Sens.* **2015**, 108, 234–244. [[CrossRef](#)]
21. L3Harris Geospatial Solutions Inc. Leaf Pigments. 2022. Available online: <https://www.l3harrisgeospatial.com/docs/leafpigments.html> (accessed on 12 September 2022).
22. Richardson, A.J.; Wiegand, C.L. Distinguishing vegetation from soil background information. *Photogramm. Eng. Remote Sens.* **1977**, 43, 1541–1552.
23. Jordan, C.F. Derivation of Leaf-Area Index from Quality of Light on the Forest Floor. *Ecology* **1969**, 50, 663–666. [[CrossRef](#)]
24. Hasegawa, S. Metabolism of limonoids. Limonin D-ring lactone hydrolase activity in *Pseudomonas*. *J. Agric. Food Chem.* **1976**, 24, 24–26. [[CrossRef](#)] [[PubMed](#)]
25. Huete, A.R. A soil-adjusted vegetation index (SAVI). *Remote Sens. Environ.* **1988**, 25, 295–309. [[CrossRef](#)]
26. Gitelson, A.A.; Kaufman, Y.J.; Merzlyak, M.N. Use of a green channel in remote sensing of global vegetation from EOS-MODIS. *Remote Sens. Environ.* **1996**, 58, 289–298. [[CrossRef](#)]
27. MAPIR CAMERA. OCN Filter Improves Results Compared to RGN Filter. 2020. Available online: <https://www.mapir.camera/pages/ocn-filter-improves-contrast-compared-to-rgn-filter> (accessed on 12 September 2022).
28. MAPIR CAMERA. How to Choose a Survey3 Camera Model. 2018. Available online: <https://www.mapir.camera/blogs/guide/how-to-choose-a-survey3-camera> (accessed on 12 September 2022).
29. Nill, K. Soy Beans: The Crop. *Encycl. Food Health* **2016**, 56–57. [[CrossRef](#)]
30. Soy Canada. Canadian Soybeans: Sustainably Grown, Customer Focused. 2022. Available online: https://soycanada.ca/wp-content/uploads/2020/06/2020_Soy_Canada_Brochure_ENG_FINALweb.pdf (accessed on 8 November 2022).

31. Diao, C. Remote sensing phenological monitoring framework to characterize corn and soybean physiological growing stages. *Remote Sens. Environ.* **2020**, *248*, 111960. [[CrossRef](#)]
32. Yue, J.; Feng, H.; Tian, Q.; Zhou, C. A robust spectral angle index for remotely assessing soybean canopy chlorophyll content in different growing stages. *Plant Methods* **2020**, *16*, 104. [[CrossRef](#)] [[PubMed](#)]
33. MAPIR CAMERA. Mapir Camera. 2023. Available online: <https://www.mapir.camera/pages/cameras> (accessed on 12 September 2022).
34. MAPIR CAMERA. Mapir Camera Control. 2023. Available online: <https://www.mapir.camera/collections/software/products/mapir-camera-control> (accessed on 10 October 2022).
35. R Studio. *The R Foundation for Statistical Computing*; R Foundation for Statistical Computing: Boston, MA, USA, 2018.
36. Nguy-Robertson, A.; Gitelson, A.; Peng, Y.; Viña, A.; Arkebauer, T.; Rundquist, D. Green Leaf Area Index Estimation in Maize and Soybean: Combining Vegetation Indices to Achieve Maximal Sensitivity. *Agron. J.* **2012**, *104*, 1336–1347. [[CrossRef](#)]
37. Gaso, D.V.; de Wit, A.; Berger, A.G.; Kooistra, L. Predicting within-field soybean yield variability by coupling Sentinel-2 leaf area index with a crop growth model. *Agric. For. Meteorol.* **2021**, *308*, 108553. [[CrossRef](#)]
38. Hoffman, J.I.E. Analysis of Variance. I. One-Way. In *Basic Biostatistics for Medical and Biomedical Practitioners*; Academic Press: Cambridge, MA, USA, 2019; pp. 391–417. [[CrossRef](#)]
39. Nettleton, D. Chapter 6—Selection of Variables and Factor Derivation. In *Commercial Data Mining*; Nettleton, D., Ed.; Morgan Kaufmann: Boston, MA, USA, 2014; pp. 79–104. [[CrossRef](#)]
40. Singh, S.K.; Hoyos-Villegas, V.; Ray, J.D.; Smith, J.R.; Fritschi, F.B. Quantification of leaf pigments in soybean (*Glycine max* (L.) Merr.) based on wavelet decomposition of hyperspectral features. *Field Crop. Res.* **2013**, *149*, 20–32. [[CrossRef](#)]
41. Gutman, G.; Skakun, S.; Gitelson, A. Revisiting the use of red and near-infrared reflectances in vegetation studies and numerical climate models. *Sci. Remote Sens.* **2021**, *4*, 100025. [[CrossRef](#)]

Disclaimer/Publisher’s Note: The statements, opinions and data contained in all publications are solely those of the individual author(s) and contributor(s) and not of MDPI and/or the editor(s). MDPI and/or the editor(s) disclaim responsibility for any injury to people or property resulting from any ideas, methods, instructions or products referred to in the content.